

Note added after first publication

This file replaces the version published on 16th January 2024. Since the first publication of this article, the Dalton Transactions Editorial Office became aware of some errors with the crystallographic data which this file rectifies, revised cif files have also been deposited with the Cambridge Crystallographic Data Centre (CCDC).

Electronic Supplementary Material (ESI) for Dalton *Transactions*.

This journal is © The Royal Society of Chemistry 2023

Supplementary Information for

**Syntheses, crystal structures and MMCT properties of the
diruthenium-based cyanido-bridged Ru₂^{V/VI}-NC-Ru^{II} complexes**

Ting-Ya Li,^{a, b} Shao-Dong Su,^a Yong He,^{a, b} Xin-Tao Wu^a and Tian-Lu Sheng^{*a}

^a State Key Laboratory of Structural Chemistry, Fujian Institute of Research on the Structure of Matter, Chinese Academy of Sciences. Fuzhou, Fujian 350002, P.R. China

^b School of Chemical Sciences, University of Chinese Academy of Sciences. Beijing, 100049, P.R. China

Table of Contents

1. Crystallographic data

Table S1: Selected bond lengths and angles of $\text{Ru}_2(\text{ap-4-Me})_3(\text{CH}_3\text{COO})\text{Cl}$ and $[\text{Ru}_2(\text{ap-4-Me})_3(\text{CH}_3\text{COO})(\text{OH})][\text{PF}_6]$

Table S2: Selected bond lengths and angles of $2[\text{PF}_6]$ and $2[\text{PF}_6]_2$

Table S3: Selected bond lengths and angles of $3[\text{PF}_6]$ and $3[\text{PF}_6]_2$

Table S4: Crystallographic data and a summary of the structural refinements for $\text{Ru}_2(\text{ap-4-Me})_3(\text{CH}_3\text{COO})\text{Cl}$ and $[\text{Ru}_2(\text{ap-4-Me})_3(\text{CH}_3\text{COO})(\text{OH})][\text{PF}_6]$

Table S5: Crystallographic data and a summary of the structural refinements for $1[\text{PF}_6]$ and $1[\text{PF}_6]_2$

Table S6: Crystallographic data and a summary of the structural refinements for $2[\text{PF}_6]$ and $2[\text{PF}_6]_2$

Table S7: Crystallographic data and a summary of the structural refinements for $3[\text{PF}_6]$ and $3[\text{PF}_6]_2$

2. Magnetic properties

Fig. S1: The magnetic susceptibility plots of complexes $\text{Ru}_2(\text{ap-4-Me})_3(\text{CH}_3\text{COO})\text{Cl}$ and $[\text{Ru}_2(\text{ap-4-Me})_3(\text{CH}_3\text{COO})(\text{OH})][\text{PF}_6]$

Fig. S2: The magnetic susceptibility plots of complexes $1[\text{PF}_6]$, $2[\text{PF}_6]$ and $3[\text{PF}_6]$

Fig. S3: The magnetic susceptibility plots of complexes $1[\text{PF}_6]_2$, $2[\text{PF}_6]_2$ and $3[\text{PF}_6]_2$

3. Electrochemical Properties

Fig. S4: Cyclic voltammograms properties of complex $2[\text{PF}_6]$ and $3[\text{PF}_6]$

Fig. S5: Cyclic voltammograms properties of complex $\text{CpRu}^{\text{II}}(\text{dppe})\text{CN}$ and $\text{CpMeRu}^{\text{II}}(\text{dppe})\text{CN}$

Fig. S6: Cyclic voltammograms properties of complex $\text{CpMe}_5\text{Ru}^{\text{II}}(\text{dppe})\text{CN}$ and $\text{Ru}_2(\text{ap-4-Me})_3(\text{CH}_3\text{COO})\text{Cl}$

4. The IR spectra

Fig. S7: The IR spectra of $2[\text{PF}_6]_n$, $3[\text{PF}_6]_n$ ($n=1, 2$) at room temperature.

Fig. S8: The IR spectra of $\text{Ru}_2(\text{ap-4-Me})_3(\text{CH}_3\text{COO})\text{Cl}$ and $[\text{Ru}_2(\text{ap-4-Me})_3(\text{CH}_3\text{COO})(\text{OH})][\text{PF}_6]$ at room temperature.

5. UV-vis-NIR spectroscopy

Fig. S9: The UV-vis-NIR spectra of complexes $\text{Ru}_2(\text{ap-4-Me})_3(\text{CH}_3\text{COO})\text{Cl}$ and $[\text{Ru}_2(\text{ap-4-Me})_3(\text{CH}_3\text{COO})(\text{OH})][\text{PF}_6]$ in CH_2Cl_2 solution

Fig. S10: The Gaussian peak fitting of the UV/Vis/NIR spectra of $2[\text{PF}_6]$ and $3[\text{PF}_6]$ in CH_2Cl_2 at room temperature.

Fig. S11: The Gaussian peak fitting of the UV/Vis/NIR spectra of $2[\text{PF}_6]_2$ and $3[\text{PF}_6]_2$ in CH_2Cl_2 at room temperature.

6. TDDFT calculations

Fig. S12: Molecular orbital diagrams for MMCT transitions of $2[\text{PF}_6]$

Fig. S13: Molecular orbital diagrams for MMCT transitions of $3[\text{PF}_6]$

Fig. S14: Molecular orbital diagrams for MMCT transitions of $2[\text{PF}_6]_2$

Fig. S15: Molecular orbital diagrams for MMCT transitions of $3[\text{PF}_6]_2$

Fig. S16: The computed spin density distribution of complexes $2[\text{PF}_6]$ and $2[\text{PF}_6]_2$

Fig. S17: The computed spin density distribution of complexes $3[\text{PF}_6]$ and $3[\text{PF}_6]_2$

Table S8: Summary of TDDFT calculations

Table S1. Selected bond lengths (Å), the distance between the metal centers (Å) and bond angle (°) of $\text{Ru}_2(\text{ap-4-Me})_3(\text{CH}_3\text{COO})\text{Cl}$ and $[\text{Ru}_2(\text{ap-4-Me})_3(\text{CH}_3\text{COO})(\text{OH})][\text{PF}_6]$

	$\text{Ru}_2(\text{ap-4-Me})_3(\text{CH}_3\text{COO})\text{Cl}$		$[\text{Ru}_2(\text{ap-4-Me})_3(\text{CH}_3\text{COO})(\text{OH})][\text{PF}_6]$	
Ru1-Ru2	2.2853(4)		2.2862(6)	
Ru1- N1	2.032(2)	2.025	1.970(5)	1.972
Ru1- N3	2.009(2)		1.965(5)	
Ru1- N5	2.036(2)		1.980(6)	
Ru2- N2	2.115(2)	2.096	2.063(5)	2.063
Ru2- N4	2.061(2)		2.048(6)	
Ru2- N6	2.112(2)		2.078(6)	
Ru1-O1	2.079(2)	2.083	2.092(5)	2.080
Ru2-O2	2.087(2)		2.068(5)	
Ru1-Cl1	2.4678(7)			
Ru1-Ru2 -Cl1	172.85(2)			

Table S2. Selected bond lengths (Å), the distance between the metal center (Å) and bond angle (°) of $2[\text{PF}_6], 2[\text{PF}_6]_2$

	$2[\text{PF}_6]$	2^+ average	$2[\text{PF}_6]_2$	2^{2+} average
Ru1-Ru2	2.2786(4)		2.3026(4)	
Ru1- N1	2.019(3)	2.013	1.977(4)	1.967
Ru1- N3	2.011(3)		1.955(4)	
Ru1- N5	2.009(3)		1.969(3)	
Ru2- N2	2.095(3)	2.085	2.090(4)	2.063
Ru2- N4	2.046(3)		2.029(4)	
Ru2- N6	2.116(3)		2.070(3)	
Ru1-O1	2.098(3)	2.096	2.097(3)	2.088
Ru2-O2	2.094(2)		2.080(3)	
Ru3-P1	2.2788(11)	2.2721	2.2676(11)	2.2775
Ru3-P2	2.2665(10)		2.2874(11)	
Ru3-C1	1.961(4)		1.923(4)	
Ru2- N7	2.166(3)		2.097(3)	
C≡N	1.164(5)		1.183(6)	
Ru2-N7-C1	145.8(3)		146.8(3)	
Ru3-C1-N7	171.0(3)		172.3(4)	

Table S3. Selected bond lengths (Å), the distance between the metal center (Å) and bond angle (°) of **3[PF₆]**, **3[PF₆]₂**

	3[PF₆]	3⁺ average	3[PF₆]₂	3²⁺ average
Ru1-Ru2	2.2859(4)		2.2978(4)	
Ru1- N1	2.044(3)	2.021	1.975(3)	1.978
Ru1- N3	2.002(3)		1.965(3)	
Ru1- N5	2.016(3)		1.993(3)	
Ru2- N2	2.097(3)	2.075	2.086(3)	2.072
Ru2- N4	2.042(3)		2.033(3)	
Ru2- N6	2.087(3)		2.096(3)	
Ru1-O1	2.077(2)	2.082	2.088(3)	2.080
Ru2-O2	2.087(3)		2.073(3)	
Ru3-P1	2.2911(10)	2.2886	2.2905(17)	2.2837
Ru3-P2	2.2862(10)		2.277(2)	
Ru3-C1	1.967(4)		1.968(4)	
Ru2- N7	2.155(3)		2.128(3)	
C≡N	1.164(5)		1.153(5)	
Ru2-N7-C1	159.1(3)		161.5(3)	
Ru3-C1-N7	176.3(3)		176.9(4)	

Table S4. Crystallographic data for **Ru₂(ap-4-Me)₃(CH₃COO)Cl** and **[Ru₂(ap-4-Me)₃(CH₃COO)(OH)](PF₆)**

	Ru₂(ap-4-Me)₃(CH₃COO)Cl	[Ru₂(ap-4-Me)₃(CH₃COO)(OH)](PF₆)
Empirical formula	C ₃₈ H ₃₆ ClN ₆ O ₂ Ru ₂	C ₃₈ H _{38.6} F ₆ N ₆ O _{3.8} PRu ₂
Formula weight	846.32	987.26
Temperature/K	298	293(2)
Crystal system	orthorhombic	triclinic
Space group	<i>Pbca</i>	<i>P</i> -1
a/Å	18.459(3)	10.5385(5)
b/Å	19.596(3)	14.2065(6)
c/Å	20.090(3)	14.4085(6)
α/°	90	93.838(3)
β/°	90	110.782(4)
γ/°	90	95.421(3)
Volume/Å ³	7267(2)	1996.07(16)
Z	8	2
ρ _{calc} /cm ³	1.547	1.643
μ/mm ⁻¹	0.947	4.829
F(000)	3416.0	992.0
Crystal size/mm ³	0.3 × 0.2 × 0.2	0.3 × 0.3 × 0.2
Radiation	MoKα (λ = 0.71073)	GaKα (λ = 1.3405)
2θ range for data collection/°	5.808 to 56.558	5.738 to 104.082
Index ranges	-24 ≤ h ≤ 24, -26 ≤ k ≤ 26, -26 ≤ l ≤ 26	-12 ≤ h ≤ 12, -14 ≤ k ≤ 16, -16 ≤ l ≤ 16
Reflections collected	86591	21253
Independent reflections	9003 [R _{int} = 0.0597, R _{sigma} = 0.0271]	6787 [R _{int} = 0.1195, R _{sigma} = 0.1074]
Data/restraints/parameters	9003/0/513	6787/24/520
Goodness-of-fit on F ²	1.184	1.043
Final R indexes [I > 2σ (I)]	R1 = 0.0386, wR2 = 0.0931	R1 = 0.0636, wR2 = 0.1667
Final R indexes [all data]	R1 = 0.0411, wR2 = 0.0950	R1 = 0.0921, wR2 = 0.1799
Largest diff. peak/hole / e Å ⁻³	0.78/-0.68	0.89/-1.13

Table S5. Crystallographic data for **1[PF₆]_n** (n = 1, 2)

	1[PF₆]	1[PF₆]₂
Empirical formula	C ₇₃ H ₇₁ Cl ₆ F ₆ N ₇ O ₂ P ₃ Ru ₃	C ₇₀ H ₆₅ F ₁₂ N ₇ O ₂ P ₄ Ru ₃ ·2CH ₂ Cl ₂
Formula weight	1765	1861.23
Temperature/K	100.00(10)	100(2)
Crystal system	triclinic	triclinic
Space group	<i>P</i> -1	<i>P</i> -1
a/Å	10.88399(16)	10.36790(10)
b/Å	17.8080(3)	13.51430(10)
c/Å	19.4153(3)	27.3364(2)
α/°	82.5338(14)	99.9230(10)
β/°	80.6957(13)	92.2530(10)
γ/°	89.2357(13)	103.0040(10)
Volume/Å ³	3682.01(10)	3663.99(6)
Z	2	2
ρ _{calc} /cm ³	1.591	1.687
μ/mm ⁻¹	5.213	5.252
F(000)	1776.0	1868.0
Crystal size/mm ³	0.5 × 0.4 × 0.2	0.4 × 0.3 × 0.3
Radiation	micro-focus metaljet (λ = 1.3405)	GaKα (λ = 1.3405)
2θ range for data collection/°	4.044 to 105.854	5.726 to 107.708
Index ranges	-12 ≤ h ≤ 12, -20 ≤ k ≤ 21, -23 ≤ l ≤ 23	-12 ≤ h ≤ 11, -14 ≤ k ≤ 16, -32 ≤ l ≤ 32
Reflections collected	19940	38602
Independent reflections	19940 [Rint = ?, Rsigma = 0.0099]	13438 [Rint = 0.0722, Rsigma = 0.0513]
Data/restraints/parameters	19940/6/958	13438/89/1028
Goodness-of-fit on F ²	1.030	1.045
Final R indexes [I ≥ 2σ (I)]	R1 = 0.0558, wR2 = 0.1541	R1 = 0.0581, wR2 = 0.1687
Final R indexes [all data]	R1 = 0.0575, wR2 = 0.1563	R1 = 0.0617, wR2 = 0.1718
Largest diff. peak/hole / e Å ⁻³	2.06/-1.60	1.94/-1.83

Table S6. Crystallographic data for **2[PF₆]_n** (n = 1, 2)

	2[PF₆]	2[PF₆]₂
Empirical formula	C _{74.4} H _{74.8} Cl _{0.8} F ₆ N ₇ O ₂ P ₃ Ru ₃	C ₇₅ H ₇₆ Cl ₂ F ₁₂ N ₇ O ₂ P ₄ Ru ₃
Formula weight	1637.49	1833.41
Temperature/K	300.01(14)	100(2)
Crystal system	triclinic	triclinic
Space group	<i>P</i> -1	<i>P</i> -1
a/Å	10.9565(3)	10.59036(15)
b/Å	15.0440(3)	13.36324(19)
c/Å	22.5663(4)	27.4852(4)
α/°	75.615(2)	100.1569(12)
β/°	81.746(2)	91.5001(12)
γ/°	86.590(2)	101.5263(12)
Volume/Å ³	3564.56(14)	3743.96(10)
Z	2	2
ρ _{calc} /cm ³	1.526	1.626
μ/mm ⁻¹	4.405	4.705
F(000)	1662.0	1850.0
Crystal size/mm ³	0.4 × 0.3 × 0.2	0.5 × 0.2 × 0.1
Radiation	Ga Kα (λ = 1.3405)	Ga Kα (λ = 1.3405)
2θ range for data collection/°	5.274 to 107.71	5.692 to 107.708
Index ranges	-13 ≤ h ≤ 13, -18 ≤ k ≤ 18, -26 ≤ l ≤ 27	-12 ≤ h ≤ 12, -16 ≤ k ≤ 16, -33 ≤ l ≤ 32
Reflections collected	46023	46448
Independent reflections	13012 [R _{int} = 0.0424, R _{sigma} = 0.0362]	13705 [R _{int} = 0.0392, R _{sigma} = 0.0343]
Data/restraints/parameters	13012/8/854	13705/0/918
Goodness-of-fit on F ²	1.035	1.051
Final R indexes [I >= 2σ (I)]	R1 = 0.0421, wR2 = 0.1109	R1 = 0.0466, wR2 = 0.1106
Final R indexes [all data]	R1 = 0.0477, wR2 = 0.1137	R1 = 0.0533, wR2 = 0.1132
Largest diff. peak/hole / e Å ⁻³	0.80/-0.78	1.87/-1.05

Table S7. Crystallographic data for **3[PF₆]_n** (n = 1,2)

	3[PF₆]	3[PF₆]₂
Empirical formula	C ₈₁ H _{89.5} Cl ₃ F ₆ N ₇ O _{2.5} P ₃ Ru ₃	C ₇₈ H ₈₂ F ₁₂ N ₇ O ₂ P ₄ Ru ₃
Formula weight	1817.56	1804.59
Temperature/K	100.00(10)	293(2)
Crystal system	triclinic	monoclinic
Space group	<i>P</i> -1	<i>C</i> 2/ <i>c</i>
a/Å	13.7545(2)	61.4094(4)
b/Å	16.2220(2)	11.13090(10)
c/Å	19.0188(2)	26.7856(2)
α/°	92.2200(10)	90
β/°	101.8150(10)	99.9850(10)
γ/°	105.3120(10)	90
Volume/Å ³	3986.82(9)	18031.8(2)
Z	2	8
ρ _{calc} /cm ³	1.514	1.329
μ/mm ⁻¹	4.412	3.490
F(000)	1853.0	7320.0
Crystal size/mm ³	0.3 × 0.2 × 0.2	0.4 × 0.4 × 0.3
Radiation	Ga Kα (λ = 1.3405)	micro-focus metaljet (λ = 1.3405)
2θ range for data collection/°	4.146 to 107.71	5.938 to 107.708
Index ranges	-16 ≤ h ≤ 16, -19 ≤ k ≤ 19, -22 ≤ l ≤ 15	-73 ≤ h ≤ 73, -13 ≤ k ≤ 13, -32 ≤ l ≤ 31
Reflections collected	41509	61780
Independent reflections	14600 [R _{int} = 0.0562, R _{sigma} = 0.0366]	16407 [R _{int} = 0.0261, R _{sigma} = 0.0196]
Data/restraints/parameters	14600/141/892	16407/180/973
Goodness-of-fit on F ²	1.046	1.075
Final R indexes [I >= 2σ (I)]	R ₁ = 0.0567, wR ₂ = 0.1521	R ₁ = 0.0564, wR ₂ = 0.1752
Final R indexes [all data]	R ₁ = 0.0580, wR ₂ = 0.1537	R ₁ = 0.0607, wR ₂ = 0.1793
Largest diff. peak/hole / e Å ⁻³	2.86/-2.27	0.72/-0.55

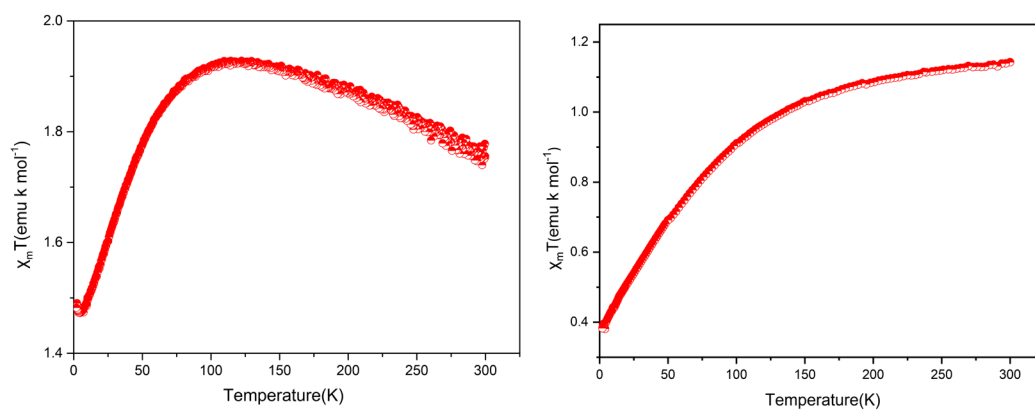


Fig.S1 Temperature dependence (2–300 K) of magnetic moments of solid sample **Ru₂(ap-4-Me)₃(CH₃COO)Cl** (left) and **[Ru₂(ap-4-Me)₃(CH₃COO)(OH)][PF₆]** (right).

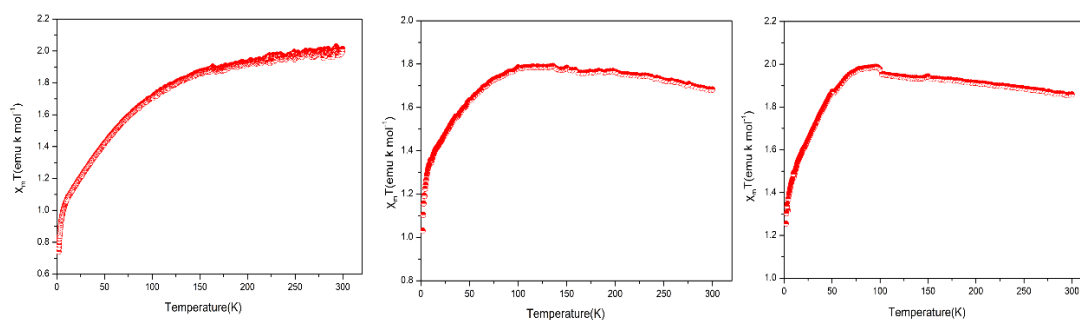


Fig. S2 Temperature dependence (2–300 K) of magnetic moments of solid sample **1[PF₆]** (left), **2[PF₆]** (middle) and **3[PF₆]** (right).

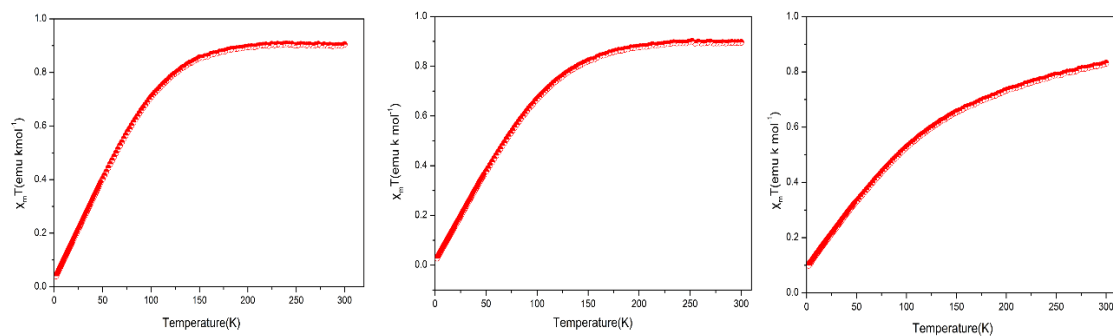


Fig. S3 Temperature dependence (2–300 K) of magnetic moments of solid sample **1[PF₆]₂** (left), **2[PF₆]₂** (middle) and **3[PF₆]₂** (right).

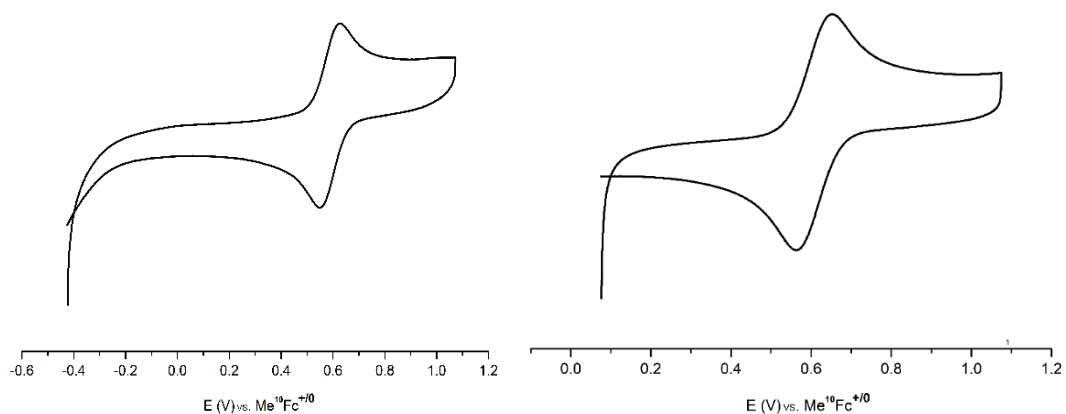


Fig. S4 Cyclic voltammograms of **2[PF₆]**, **3[PF₆]** in a 0.1 M dichloromethane solution of Bu₄NPF₆ at a scan rate of 100 mV S⁻¹ at room temperature.

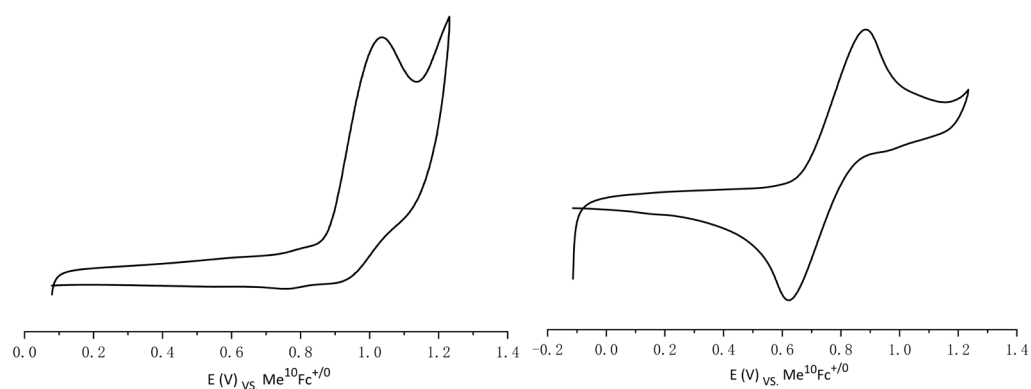


Fig. S5 Cyclic voltammograms of **CpRu^{II}(dppe)CN** (left) and **CpMeRu^{II}(dppe)CN** (right) in a 0.1 M dichloromethane solution of Bu₄NPF₆ at a scan rate of 100 mV S⁻¹ at room temperature.

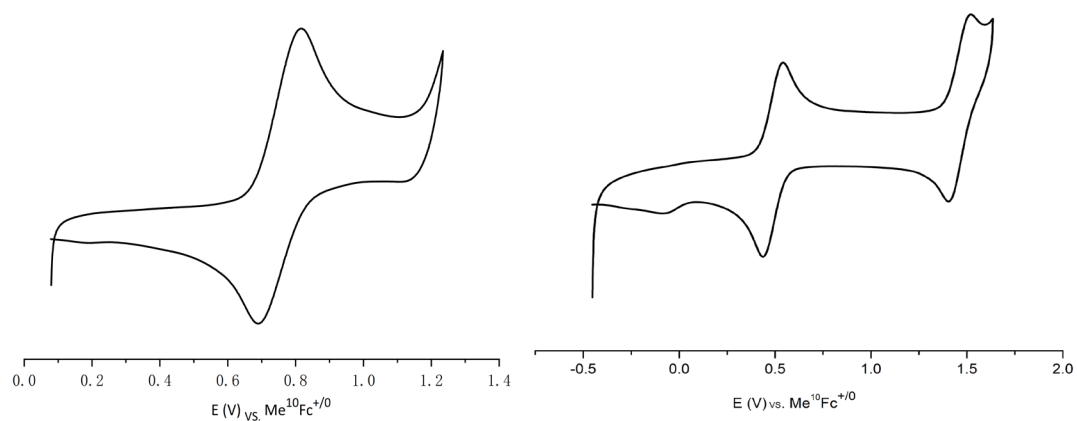


Fig. S6 Cyclic voltammograms of **CpMe₅Ru^{II}(dppe)CN** (left) and **Ru₂(ap-4-Me)₃(CH₂COO)Cl** (right) in a 0.1 M dichloromethane solution of Bu₄NPF₆ at a scan rate of 100 mV S⁻¹ at room temperature.

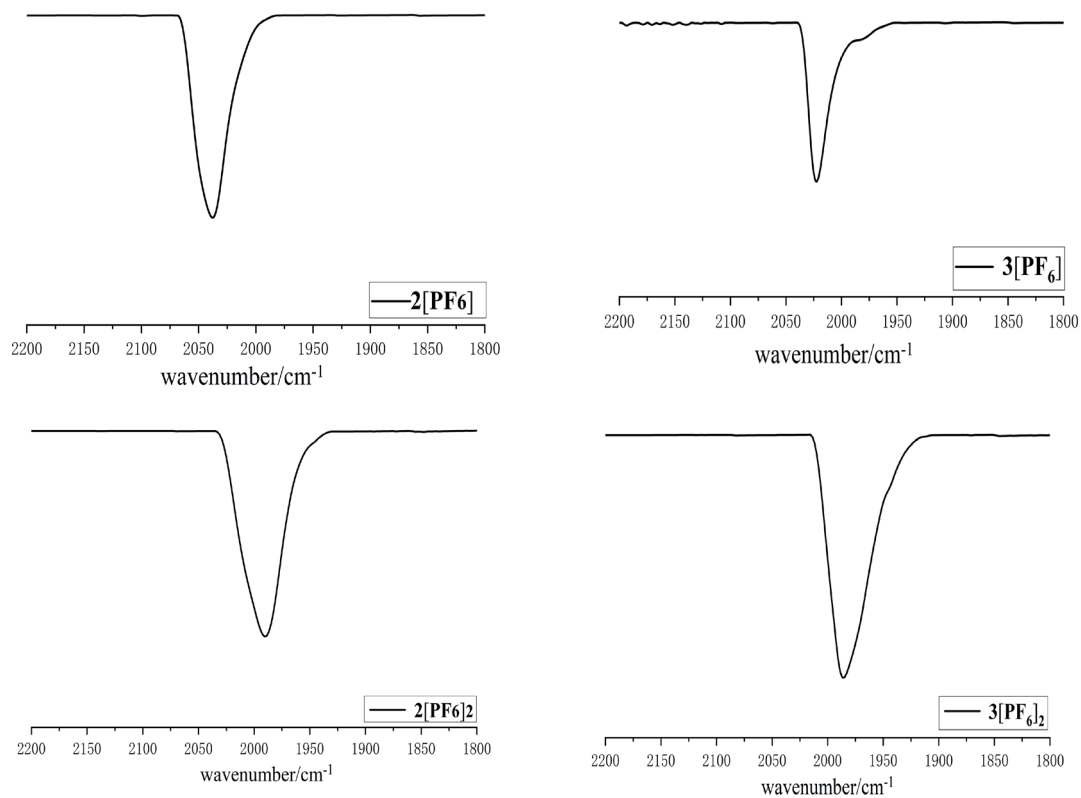


Fig S7. IR spectra of $2[\text{PF}_6]_n$, $3[\text{PF}_6]_n$ ($n=1, 2$) at room temperature.

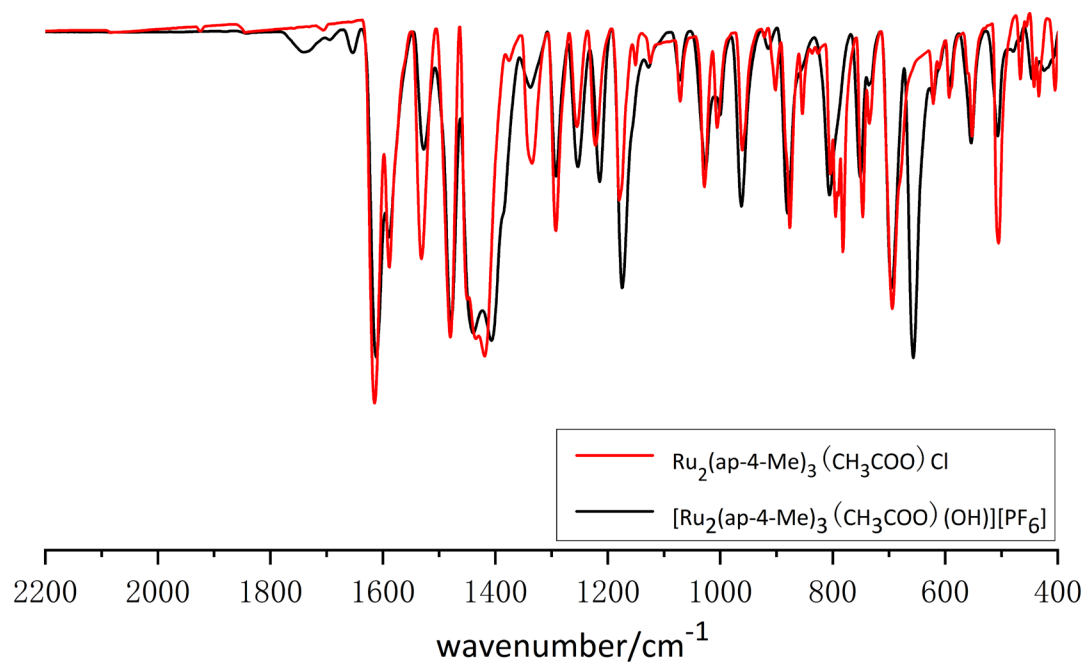


Fig S8. IR spectra of $\text{Ru}_2(\text{ap-4-Me})_3(\text{CH}_3\text{COO})\text{Cl}$ and $[\text{Ru}_2(\text{ap-4-Me})_3(\text{CH}_3\text{COO})(\text{OH})][\text{PF}_6]$ at room temperature.

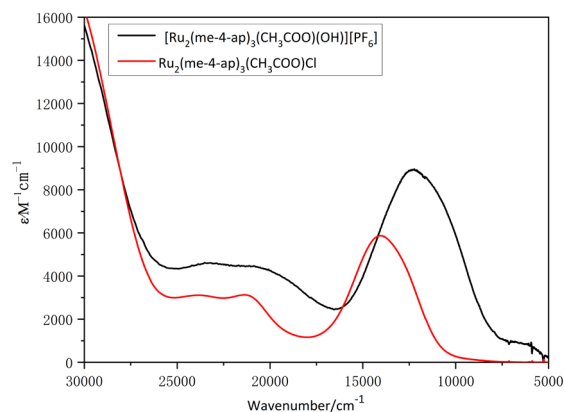


Fig. S9 UV/Vis/NIR spectra of complexes **Ru₂(ap-4-Me)₃(CH₃COO)Cl** and **[Ru₂(ap-4-Me)₃(CH₃COO)(OH)][PF₆]** in CH₂Cl₂ solution.

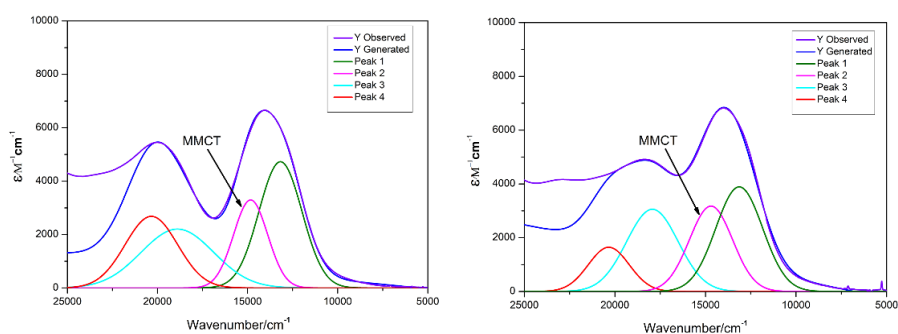


Fig. S10 The Gaussian peak fitting of the UV/Vis/NIR spectra of **2[PF₆]** and **3[PF₆]** in CH₂Cl₂ at room temperature.

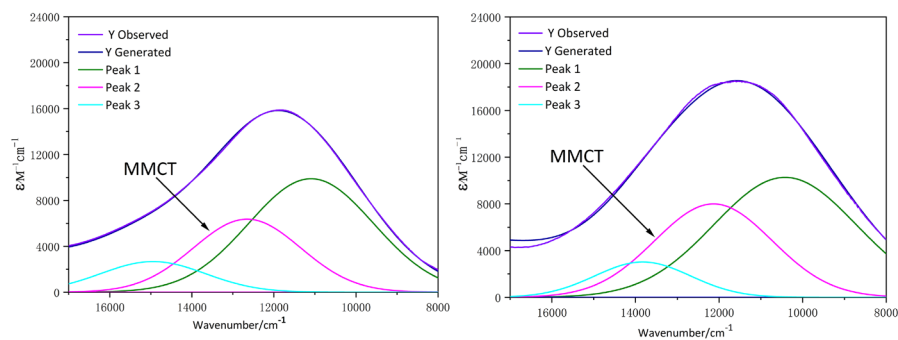


Fig. S11 The Gaussian peak fitting of the UV/Vis/NIR spectra of **2[PF₆]₂** and **3[PF₆]₂** in CH₂Cl₂ at room temperature.

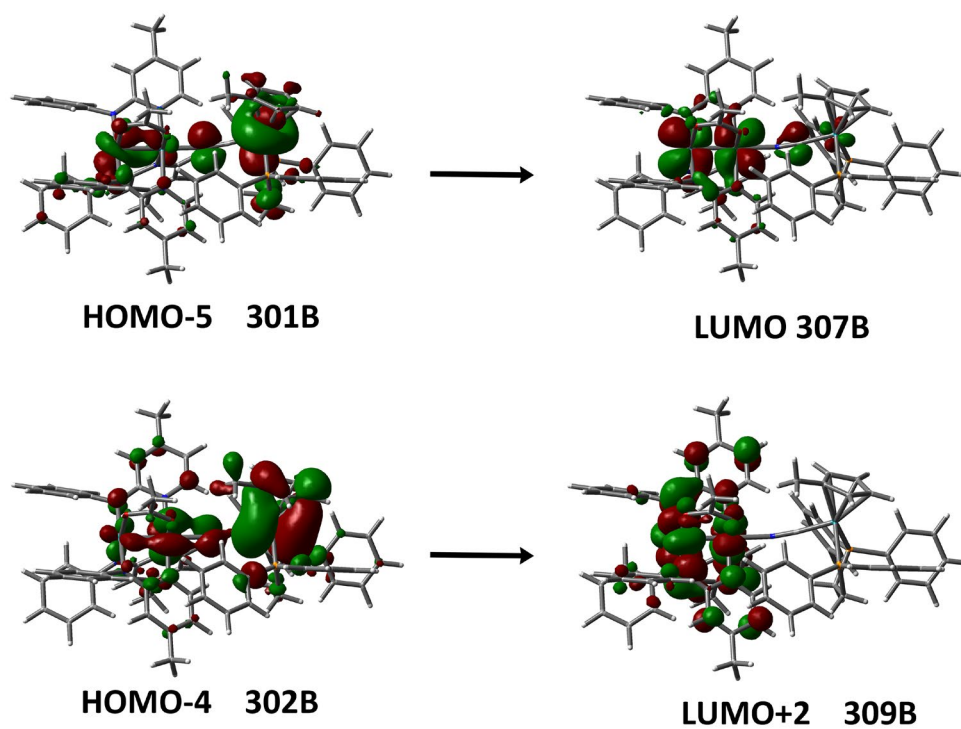


Fig. S12 Molecular orbital diagrams of HOMO-5 (301B), HOMO-4 (302B), LUMO (307B) and LUMO+2 (309B) of **2[PF₆]** in dichloromethane.

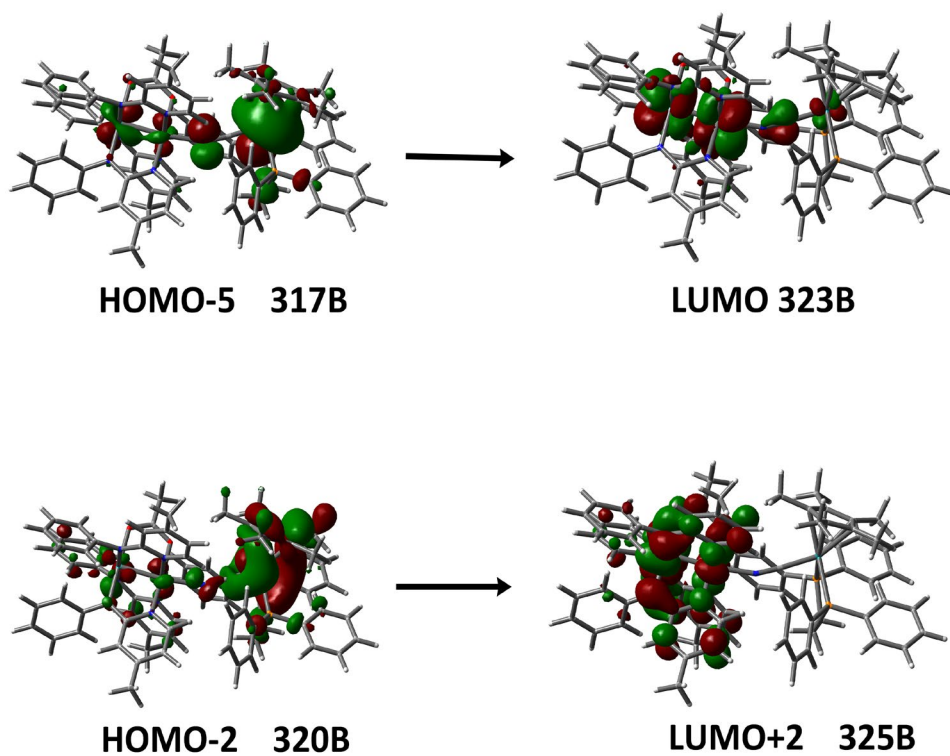


Fig. S13 Molecular orbital diagrams of HOMO-5 (317B), HOMO-2 (320B), LUMO (323B) and LUMO+2(325B) of **3[PF₆]** in dichloromethane.

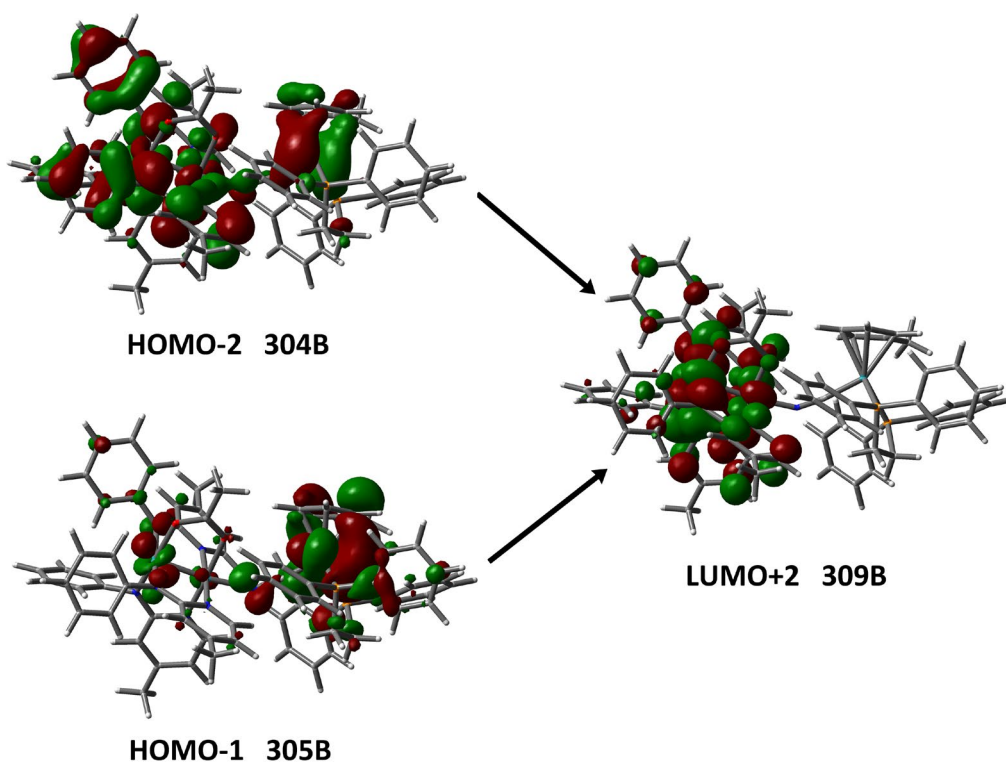


Fig. S14 Molecular orbital diagrams of HOMO-2 (304B), HOMO-1(305B), LUMO+2 (309B) of $2[\text{PF}_6]_2$ in dichloromethane.

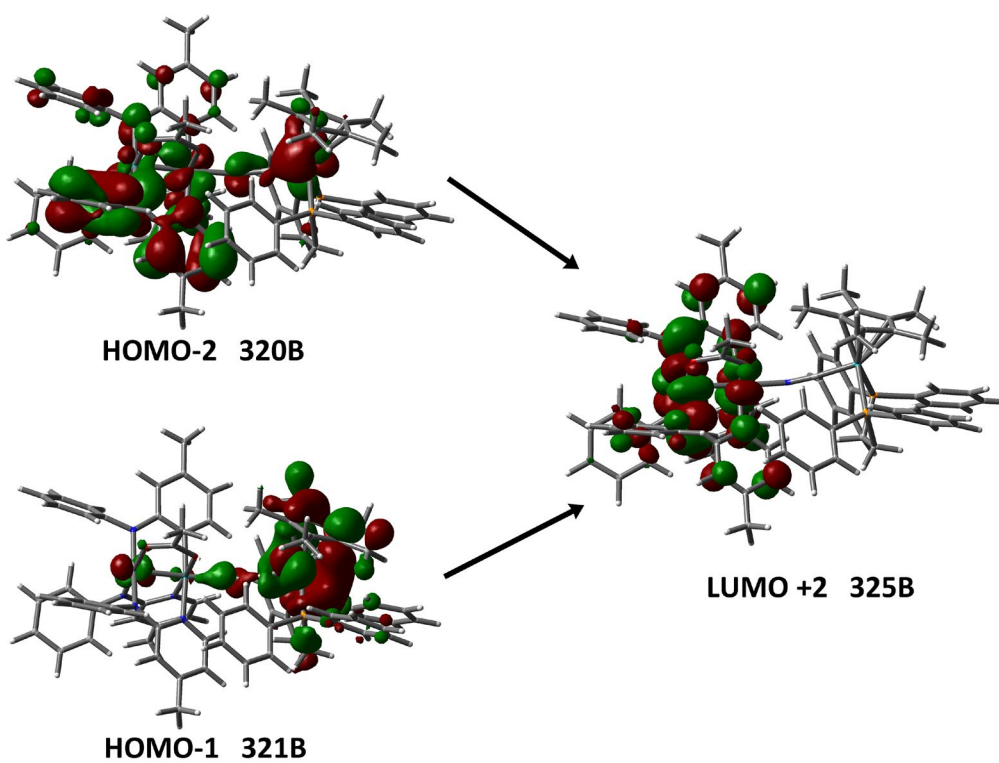


Fig. S15 Molecular orbital diagrams of HOMO-2 (320B), HOMO-1 (321B), and LUMO+2 (325B) of $3[\text{PF}_6]_2$ in dichloromethane.

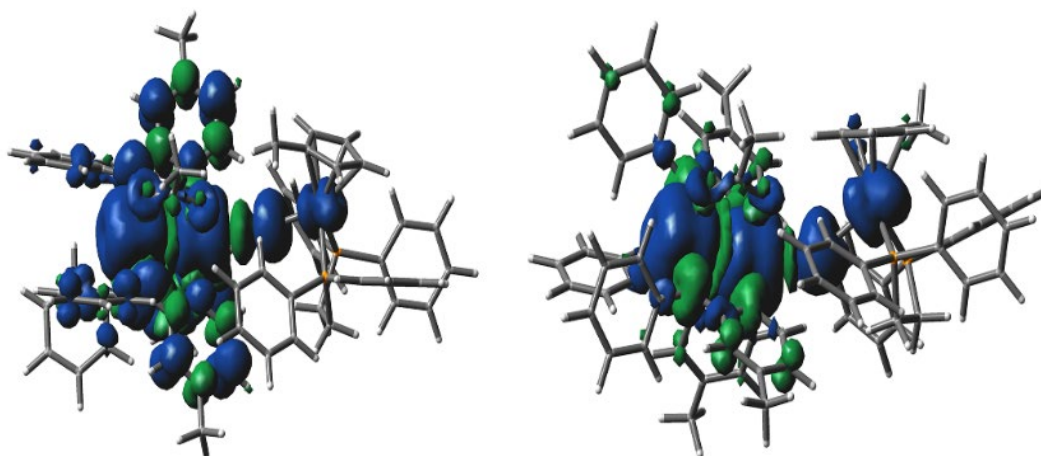


Fig. S16 The spin density distribution of $2[\text{PF}_6]$ (left), $2[\text{PF}_6]_2$ (right).

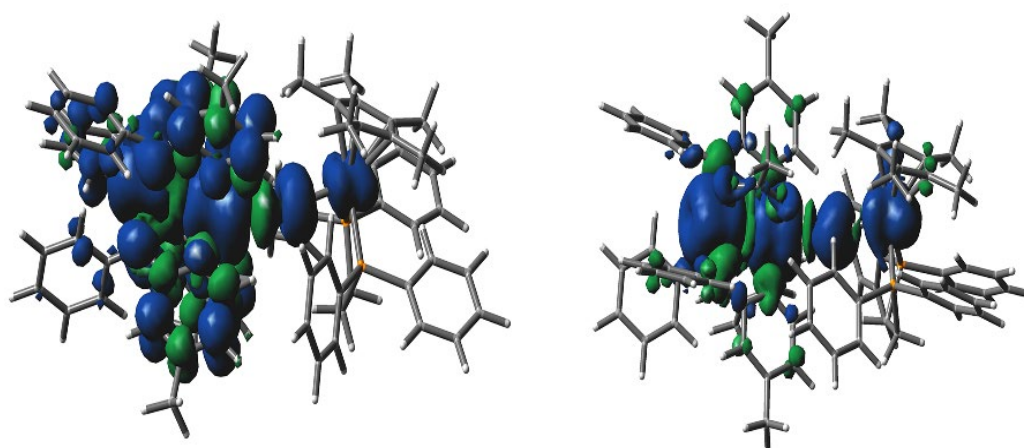


Fig. S17 The spin density distribution of $3[\text{PF}_6]$ (left), $3[\text{PF}_6]_2$ (right).

Table S8 Calculated and experimental electronic transition absorption bands of complexes $1[\text{PF}_6]_n, 2[\text{PF}_6]_n$ and $3[\text{PF}_6]_n$ ($n=1,2$)

Complex	Molecular orbital	f	$\nu_{\text{max}}(\text{exp})/\text{cm}^{-1}$	$\nu_{\text{max}}(\text{cal})/\text{cm}^{-1}$
$1[\text{PF}_6]$	HOMO-7 (295B) \rightarrow LUMO+2 (305B)	0.0185	14888	19801
	HOMO-6 (296B) \rightarrow LUMO+2 (305B)			
	HOMO-5 (297B) \rightarrow LUMO+1 (304B)			
$1[\text{PF}_6]_2$	HOMO-4 (298B) \rightarrow LUMO+2 (305B)	0.0189	12897	15015
	HOMO-2 (300B) \rightarrow LUMO+2 (305B)			
$2[\text{PF}_6]$	HOMO-5 (301B) \rightarrow LUMO (307B)	0.0329	14831	20000
	HOMO-4 (302B) \rightarrow LUMO+2 (309B)			
$2[\text{PF}_6]_2$	HOMO-1 (305B) \rightarrow LUMO+2 (309B)	0.0382	12654	14858
	HOMO-2 (304B) \rightarrow LUMO+2 (309B)			
$3[\text{PF}_6]$	HOMO-2 (320B) \rightarrow LUMO+2 (325B)	0.0227	14696	19011
	HOMO-5 (317B) \rightarrow LUMO (323B)			
$3[\text{PF}_6]_2$	HOMO-2 (320B) \rightarrow LUMO+2 (325B)	0.0329	12134	13623
	HOMO-1 (321B) \rightarrow LUMO+2 (325B)			

